SO_2 tolerance and regeneration of $Ba_{0.9}A_{0.1}Ti_{0.8}Cu_{0.2}O_3$ (A= Sr, Ca, Mg) LNT catalysts.

Vicente Albaladejo-Fuentes, María-Salvadora Sánchez-Adsuar, María-José Illán-Gómez*

Carbon Materials and Environment Research Group, Department of Inorganic Chemistry, Faculty of Science, Universidad de Alicante, Alicante, Spain

** corresponding author: illan@ua.es. Phone: +34965903975.*

Department of Inorganic Chemistry, Faculty of Science, Universidad de Alicante, Av. Alicante s/n, 03690, San Vicente del Raspeig, Alicante, Spain

ABSTRACT

In this paper, the tolerance and stability versus SO_2 of $Ba_{0.9}A_{0.1}Ti_{0.8}Cu_{0.2}O_3$ (A = Sr, Ca, Mg) perovskite-type catalysts for NOx storage application have been analyzed at 400ºC. Characterization results show that only strontium and magnesium are introduced into the perovskite structure. From those data, it can be concluded that the incorporation of Sr into the $Ba_{0.9}Sr_{0.1}Ti_{0.8}Cu_{0.2}O_3$ catalyst promotes the generation of higher amount of NOx adsorption active sites compared to the former $BaTi_{0.8}Cu_{0.2}O_3$ perovskite. On the contrary, for $Ba_{0.9}Mg_{0.1}Ti_{0.8}Cu_{0.2}O_3$ catalyst, copper is segregated from the catalyst lattice to the surface due to the incorporation of magnesium into the B site of the perovskite.

The partial substitution of barium in $Ba_{0.9}Sr_{0.1}Ti_{0.8}Cu_{0.2}O_3$ and $Ba_{0.9}Mg_{0.1}Ti_{0.8}Cu_{0.2}O_3$ catalysts leads to increases the NOx Storage Capacity (460 and 415 μmol/g.cat. in saturation conditions, respectively), stability and tolerance versus SO_2 compared to the raw $BaTi_{0.8}Cu_{0.2}O_3$ perovskite.

Keywords:

LNT catalysts, perovskite, copper, NOx storage, SO_2 tolerance

1. INTRODUCCIÓN.

Direct-injection spark ignition engines (DISI) are a lean burn engine alternative to diesel engines because of their low fuel consumption and, for hence, their low CO_2 emissions level [1]. Nevertheless, it has been reported that DISI engines increase the NOx and particulate matter (PM) emissions [2] compared to spark ignition (SI) engines [3]. The operating mode of a DISI engine (lean burn condition) prevents the complete abatement of NOx emissions by the TWC used for SI engines, and for this reason, the addition of a de-NOx after-treatment system in the exhaust is mandatory [4,5]. Two technologies are mainly proposed to control NOx emission in lean burn engines: Selective Catalytic Reduction (SCR) and "Lean NOx Trapping" (LNT) [6,7]. The conventional LNT catalysts, fitted in diesel cars, are composed of platinum-group metals (PGM) and alkaline or alkaline-earth oxides (BaO or K_2O), both supported on a high surface area material (Al_2O_3, TiO_2…) [8]. Recently, it has been demonstrated that interesting results for NOx emissions control in a DISI engine can be achieved by combining LNT and TWC technologies. However, some issues must be still addressed to match these technologies, such as: i) enhancing the NOx storage capacity of the conventional LNT catalyst at high temperature, as working range temperature for DISI engines is higher than for diesel engines [9] and ii) improving the sulfur tolerance and regeneration of the catalyst, without losing NOx storage capacity [10].

Perovskites oxides (ABO_3) are currently proposed as a promising alternative to the PGM catalyst for NOx abatement due to their high thermal stability, low cost and easy control of their catalytic and redox properties by partial substitution of A and/or B cations [11,12]. Li et al [13] suggested perovskites as LNT catalysts as they show catalytic performance close to that reported for Platinum Group Metal (PGM) catalysts, and even higher sulfur tolerance. Kim et al [14] concluded that lanthanum-based perovskites can be considered viable automotive catalysts, reaching the maximum NOx conversion at 400ºC, even though the addition of a smaller amount of a PGM is mandatory to fulfill the sulfur resistance required. In addition, Shen et al [15] and Righini et al [16], studied the stability of potassium titanates as NOx adsorbents and

concluded that the incorporation of potassium shifts the NOx adsorption to higher temperatures, though the mobility and reactivity of potassium at the required working temperatures made this catalyst not suitable for LNT application. Therefore, in spite of all these studies, more efforts have to be done to improve the NOx conversion and sulfur tolerance and regeneration before perovskites are ready to be used as LNT catalysts at high temperature.

In previous articles, the authors concluded that by partial substitution of Ti by Cu, the $BaTi_{0.8}Cu_{0.2}O_3$ perovskite becomes active for NOx storage in the temperature range of the lean burn engines application [17,18]. According to these results, and to try to overcome some of the drawbacks of LNT catalysts above-mentioned, the aim of this paper is to determine the effect of partial substitution of the A cation on the NOx storage capacity and sulfur tolerance of the $BaTi_{0.8}Cu_{0.2}O_3$ perovskite. Considering literature reviewed: i) strontium and calcium doping may enhance sulfur tolerance of a commercial LNT catalyst [19] as the corresponding sulfates, that block the NOx storage sites, are easily regenerated; ii) magnesium, as textural promoter, may improve the resistance to sintering [20,21], since the use of reducing environments during regeneration processes could lead to a collapse of the perovskite structure and, for hence, to a loss of activity [14,22,23]. Therefore, in this paper, the effect of the partial substitution of barium by strontium, calcium or magnesium in the performance of $BaTi_{0.8}Cu_{0.2}O_3$ catalyst has been analyzed.

2. EXPERIMENTAL SECTION.

2.1. Catalysts synthesis and characterization.

$Ba_{0.9}A_{0.1}Ti_{0.8}Cu_{0.2}O_3$ catalysts (A = Sr, Ca, Mg) were prepared by the modified Pechini's sol-gel method in aqueous media described elsewhere [17,18]. In brief, a 0.1M citric acid solution with 1:2 molar ratio with respect to titanium was prepared and heated up to 60 ºC. Titanium isopropoxide was hydrolyzed and the resulting solid species were filtered and dissolved in the citric acid solution. The pH of the resultant solution was increased to 8.5 by drop wising ammonia solution. Afterwards, the stoichiometric amounts of barium, copper and calcium, magnesium or strontium precursors were added to the solution in this order. Once the precursor salts were

dissolved, the pH value was readjusted to 8.5 with ammonia. The solution was kept at 65 ºC for 5h and dried at 90 ºC for 24h. The dried gel was heated up to 850 ºC at 5ºC/min and that temperature was hold for 6h.

The BET surface area of the catalysts was determined by N_2 adsorption at -196ºC in a Autosorb-6B equipment from Quantachrome. Samples were previously degasified at 250ºC for 4h.

Copper, strontium, calcium and magnesium contents were measured by ICP-OES, using a Perkin-Elmer, model Optima 4300 DV, device. Metals were extracted by solving the samples in 8M HCl (refluxing for 2h).

XRD patterns were obtained using a Bruker D8-Advance device and recorded between 20-80º 2Θ angles with a step rate of 0.02º/3s and CuKα (0.15418 nm) radiation.

XPS spectra were registered using a K-Alpha Photoelectron Spectrometer by Thermo-Scientific with an Al Kα (1486.6 eV) radiation source. For the analysis, a $5x10^{-10}$ mbar pressure was kept in the chamber. Binding energy (BE) scales were adjusted by setting C1s transition at 284.6 eV, and the BE values were then determined with the peak-fit software of the spectrometer.

The Temperature Programmed Reduction with H_2 (H_2-TPR) experiments were carried out in a Pulse Chemisorb 2705 device from Micromeritics, which is fitted with a TCD to determine the outlet gas composition. For the experiments, 20 mg of the sample were heated at 10ºC/min from room temperature to 900ºC in 5% H_2/Ar atmosphere (40 ml/min, Pt = 1 atm). The H_2 consumption was quantified using a CuO sample supplied by Micromeritics as a reference.

Temperature Programmed Desorption of Oxygen experiments (O_2- TPD) were carried out by heating 30 mg of the catalysts in a quartz reactor at 10ºC/min from 25 to 900ºC under a He flow (100 ml/min, P_{total} = 1 atm). Previously, the sample was pretreated by isothermal oxidation with a 5% O_2/He atmosphere at 500ºC for 1h. A Quadrupole Mass Spectrometer (Pfeiffer Vacuum model Thermostar) was used to monitor gas composition during the O_2-TPD experiments.

Infrared spectroscopy analysis of the fresh and used samples was done using a JASCO FT/IR 4100 spectrometer with and MTC detector and fitted with a Harrick's Praying Mantis diffuse reflection accessory. DRIFTS spectra were recorded in the 5000-500 cm^{-1} wavenumber range with a 4 cm^{-1} resolution and as an average of 40 scans.

2.2. Catalytic activity tests.

The NOx storage capacity (NSC) of the catalysts was determined by NOx storage-regeneration cyclic (NSRC) experiments at 400ºC. The NSRC experiments were carried out in a fixed bed reactor (80 mg of catalyst diluted in 320 mg SiC) and using a total gas flow of 500 ml/min composed by: i) 500 ppm NO + 5% O_2 balanced with N_2 for the lean cycle (5 min) and ii) 10% H_2 in N_2 balance for the rich cycle (3 min), used for ensuring the total catalyst regeneration. The effect of SO_2 on the NSC was analyzed by carrying out analogous NSRC experiments but using a 500 ppm NO + 100 ppm SO_2 + 5% O_2 balanced with N_2 during the lean cycle. The amount of SO_2 added to the gas flow implies that the catalysts were exposed every lean cycle to 4 mg. S/g. cat., which is a load of sulfur larger than the corresponding to real conditions [24, 25]. Ten consecutive storage-regeneration cycles were performed in order to achieve the catalysts stability [17, 18].

NOx saturation experiments were carried out in absence and presence of SO_2, as follows: fresh catalysts were conditioned by carrying out three NOx storage-regeneration cycles at 400ºC to ensure a stable behavior and, afterward, they were exposed to a 1 hour long NOx adsorption cycle using a total gas flow of 500 ppm NO + 5% O_2 balanced with N_2 or 500 ppm NO + 100 ppm SO_2+ 5% O_2 balanced with N_2 atmosphere.

For the analysis of the SO_2 regeneration of the catalysts, the procedure detailed in Table 1 was followed. Briefly, 20 consecutive storage-regeneration cycles were carried out: i) during the 5 first cycles a NO/O_2 atmosphere was used for lean cycle to determine the NSC of the fresh catalyst, ii) in the next 5 cycles, the catalysts were poisoned due to the introduction of SO_2 in the lean cycle atmosphere and, finally, iii) 10 storage-regeneration cycles were carried out without feeding SO_2 during the lean cycle.

The gas composition during the experiment was monitored by specific NDIR-UV gas analyzers for NO, NO_2, CO, CO_2, SO_2 and O_2 (Rosemount Analytical Model BINOS 1001, 1004 and 1000). The NSC was calculated as the difference between the NOx concentration when the reactor is empty and the NOx concentration in the presence of the catalyst:

$$NSC = \int_{t_0}^{t_f} NO_{X,inlet}(t) - NO_{X,exp}(t)dt \qquad (1)$$

where "NOx, inlet" is the concentration of NOx (=NO + NO_2) measured for the empty reactor, and "NOx, exp", is the concentration of NOx during the lean cycles.

3. RESULTS AND DISCUSSION.

3.1. Characterization of fresh catalysts.

The actual metal content of the $Ba_{0.9}A_{0.1}Ti_{0.8}Cu_{0.2}O_3$ catalysts (determined by ICP-OES and featured in Table 2, where also the catalysts nomenclature and the specific surface area are shown) confirms the incorporation of almost all the nominal amount of A and Cu metals into the catalysts. The specific surface area of the catalysts (measured by N_2-adsorption) reveals that all the perovskite show almost negligible porosity, as it is expected for these mixed oxides [22].

3.1.1. Structural properties.

XRD difractograms shown in Figure 1, point out perovskite structure as the main phase for all the $Ba_{0.9}A_{0.1}Ti_{0.8}Cu_{0.2}O_3$ catalysts regardless the A and/or the B cations substitution. The XRD pattern of a $BaTiO_3$ mixed oxide (BTO), prepared following the same synthesis method, is also included as a reference. From the comparison of the BTO and BTCuO, BTCuO_Sr and BTCuO_Mg patterns it can be observed that there are some differences on the minority phases identified for these perovskites. In this respect, only $BaCO_3$ is identified as secondary phase in BTO, whilst other minority species such as Ba_2TiO_4, and CuO are observed in the copper content catalysts. Thus, in agreement with previous results [17, 18], it can be concluded that strontium, magnesium, and copper are totally or partially incorporated into the perovskite structure. For BTCuO_Ca catalyst diffraction peaks ascribed to CuO and to a new

barium-calcium titanate phase ($Ba_2Ca_2Ti_2O_8$) are identified, suggesting that calcium and copper are scarcely incorporated into the perovskite lattice. This result would be expected based on the large difference between the ionic radii of Ca (II) (134 pm) and Ba (II) (141 pm).

In Figure 1b, the 2Θ diffraction angle area corresponding to the main peak of the $BaTiO_3$ perovskite structure has been enlarged. In this figure, it is observed a shift in the of the mean perovskite peak to a higher diffraction angle for BTCuO and, more pronounced, for BTCuO_Sr catalysts compared to BTO reference catalyst. Zhang et al [26] also observed a slight shift of the main peak of the $CaTiO_3$ perovskite when copper was added to the formulation, concluding that copper had been introduced into the lattice by replacing Ti (IV) in B sites, since a replacement of Ca (II) by Cu (II) would lead to a larger shift in the peak position. Besides, the effect of strontium substitution in barium titanate mixed oxides has been widely studied and it is accepted that A site replacement causes a distortion of the structure, involving a pronounced shift of the diffraction peaks [27-29]. Therefore, the distortion of the original perovskite structure allows concluding that copper is satisfactorily incorporated into BTCuO and BTCuO_Sr perovskite, and, also, that the distortion is more pronounced for BTCuO_Sr catalyst due to the additional introduction of strontium. As for the BTCuO_Ca and BTCuO_Mg catalyst the shift in the position of the main peak is not observed, it seems that calcium and magnesium are not incorporated into the A position of the perovskite structure. Nevertheless, Fu and co-workers [30] concluded that a solid solution of calcium and barium titanate was possible, even at a high calcium concentration, without distortion of the $BaTiO_3$ tetragonal structure. Therefore, in spite of the calcium-barium oxides segregation detected in the XRD pattern of BTCuO_Ca catalysts, a partial incorporation of calcium into the structure should not be completely excluded. In the case of the BTCuO_Mg catalyst, some studies about magnesium doping of barium strontium titanates [31–33] concluded that, at high magnesium content, Mg (II) replaces Ti (IV) in B sites of the perovskite instead Ba(II) in the A sites. Thus, it is proposed that the incorporation of magnesium into the $Ba_{0.9}A_{0.1}Ti_{0.8}Cu_{0.2}O_3$ perovskite is achieved, but

with Mg (II) replacing Ti(IV) or Cu(II) in 6-coordinated (B) sites instead in the 12-coordinated (A) sites replacing Ba(II).

By XRD characterization, the tetragonal structure of the perovskites can be identified as a doublet peak at 45º corresponding to the (0 0 2) and (2 0 0) diffraction peaks [17, 18], even though, a high crystallinity degree is required. Anyway, by comparing the FWHM of the (1 1 1) and (2 0 0) peaks, the cubic or tetragonal structure could be also determined: a FWHM (2 0 0) / FWHM (1 1 1) ratio value greater than 1 would be expected for a tetragonal structure (due to (0 0 2) and (2 0 0) peaks overlapping) and lower than 1 for a cubic one [17, 18]. Table 3 features the values which allows concluding that all $Ba_{0.9}A_{0.1}Ti_{0.8}Cu_{0.2}O_3$ catalysts show tetragonal structure, since all the ratios are higher than 1. However, the low ratio observed for the BTCuO_Sr (1.21) and, especially, BTCuO_Mg (1.05) catalysts (compared to the BTO catalyst used as a reference (1.76)) suggest a pseudotransition from tetragonal to cubic structure for strontium and, more clearly, for magnesium. Using the (1 1 0) and (1 1 1) peaks, at 31.5º and 39º respectively, the lattice parameters *a* and *c*, corresponding to tetragonal structure were calculated being the values included in Table 3. Comparing the c/a ratios with those of the BTO catalyst used as a reference (Figure S1 in Supplementary Information), an increase for all the $Ba_{0.9}A_{0.1}Ti_{0.8}Cu_{0.2}O_3$ catalysts is observed reaching or exceeding the value of 1 (which is the value expected for a cubic structure) for BTCuO, BTCuO_Sr and BTCuO_Mg catalysts. Thus, the c/a ratio values confirm that copper, strontium and magnesium incorporation into the mixed oxide framework provokes that the perovskite structure changes from the bare tetragonal structure to a cubic one.

3.1.2. Surface and redox properties.

XPS gives valuable information about the copper and oxygen species present on the surface of the $Ba_{0.9}A_{0.1}Ti_{0.8}Cu_{0.2}O_3$ perovskite. Figure 2 shows the XPS spectra for Cu $2p_{3/2}$ and O1s transitions.

The deconvolution of the XPS profiles corresponding to the Cu $2p_{3/2}$ transition (Figure 2a) shows two contributions, with maxima at ≈ 933 eV and ≈ 935 eV, and a

"shake-up" peak, at ≈ 942 eV which can be assigned to Cu (II) species [34]. The Cu/(Ba + A + Ti + Cu) ratio, calculated from the surface atomic percentages determined by XPS and included in Table 3, supports that copper is introduced into the perovskite structure as the XPS ratios are lower than the nominal ratio (0.10). For BTCuO_Sr and BTCuO_Mg, the Cu/(Ba + A + Ti + Cu) ratio is higher than for the BTCuO, indicating a copper segregation towards the catalyst surface. This fact suggests that the replacement of barium by strontium makes more difficult the insertion of copper into the perovskite structure and, consequently, a lower copper insertion is achieved. For BTCuO_Mg, the value of the Cu/(Ba + A + Ti + Cu) ratio supports that Mg (II) is replacing Cu (II) in B sites instead of Ti (IV), to avoid a huge distortion of the structure, as it was above suggested based on the low structure distortion observed by X-Ray diffraction.

Figure 2b shows the XPS spectra obtained for the O1s transition, where three different contributions are observed at 529, 531 and 533.5 eV, corresponding to lattice oxygen of metal oxides (O_L), adsorbed oxygen species (O*), such as surface carbonates and/or hydroxyl groups, and adsorbed water (O_{H2O}), respectively [35]. For all the A doped catalysts, the area of the bands corresponding to adsorbed oxygen species (O*) increases compared to BTCuO, indicating that the incorporation of the new A cation generates larger amounts of defects on the catalyst surface. The O_L/(Ba + A + Ti + Cu) ratio (Table 3), calculated from the peak area of O_L (lattice oxygen), $Ti2p_{3/2}$, $Ba3d_{3/2}$ and $Cu2p_{3/2}$ transitions, shows that the generation of oxygen vacancies on the perovskite structure depends on the A cation substitution. In fact, the XPS O_L/(Ba + A + Ti + Cu) ratio decreases when copper is introduced into the structure, but drops again when magnesium, calcium and strontium are incorporated confirming that, by A doping, additional oxygen defects are generated in the structure.

In order to support this observation, oxygen Temperature Programed Desorption (O_2-TPD) experiments were carried out for all the $Ba_{0.9}A_{0.1}Ti_{0.8}Cu_{0.2}O_3$ catalysts, and the normalized m/z = 32 signals recorded are shown in Figure 3. The O_2-TPD profiles of the BTCuO, BTCuO_Sr and BTCuO_Mg catalysts feature two peaks at different temperature that, accordingly to literature [35,36], can be ascribed to the desorption of

surface adsorbed oxygen (α-O_2 at low temperature) and to the desorption of oxygen from the perovskite lattice (β-O_2 at high temperature). Note that the intensity of the α-O_2 peak increases for BTCuO_Sr and BTCuO_Mg compared to BTCuO, which indicates that these catalysts show higher oxygen adsorption capacity. Considering that this peak is directly associated with the amount of oxygen defects on the catalysts, this result supports that the partial substitution of barium generates additional oxygen defects in the structure. Additionally, beyond 750ºC, high-intensity m/z = 28 and m/z = 44 signals ascribed to the desorption of CO and CO_2 (not shown for the sake or brevity) are also recorded for all the catalysts due to the decomposition of $BaCO_3$, also identified by XRD and XPS.

Figure 4 shows the H_2 consumption profiles recorded by Temperature Programmed Reduction with hydrogen (H_2-TPR) for all the $Ba_{0.9}A_{0.1}Ti_{0.8}Cu_{0.2}O_3$ catalysts. All the H_2 consumption profiles present two quite well-defined peaks between 250 and 450ºC ascribed to the reduction of copper species. Based on the area of these peaks, the molar percentage of copper reduced has been calculated and included in Table 3. The data indicate that almost all the copper species have been reduced during the experiment, except for BTCuO_Sr. The presence of two reduction peaks indicate that two copper species with different reducibility exist on the catalysts [17, 18]: i) the most intense peak corresponding to copper incorporated into the lattice or with a strong electronic interaction with the perovskite, and for hence more easily reducible and ii) the less intense peak which is associated to surface copper species as its reducibility is close to that of the CuO used as reference. Based on the H_2-TPR profiles, it seems that the reducibility of the catalysts decreases as BTCuO > BTCuO_Sr > BTCuO_Ca > BTCuO_Mg. Note that, for the BTCuO, BTCuO_Ca and BTCuO_Mg catalysts the peak corresponding to the reduction of surface CuO appears as a shoulder of the main reduction peak whilst, for the BTCuO_Sr catalyst, both peaks are clearly defined. This fact and the lower percentage of copper reduced on BTCuO_Sr surface, suggests that the simultaneous substitution of strontium and copper in A and B sites, respectively, decreases the copper - perovskite surface interaction and, for hence, the copper reducibility [17, 18]. Finally, for the BTCuO, BTCuO_Sr and BTCuO_Mg catalysts, a

low intensity peak beyond 500ºC due to desorption of oxygen surface species (such as adsorbed oxygen species identified by O_2-TPD and or carbonates by both XPS and XRD) is observed.

3.2. Catalytic activity.

3.2.1. NOx Storage Capacity (NSC) and NOx saturation experiments.

In order to study the effect of the A cation substitution on the activity, NSRC experiments at 400ºC were carried out, being the NSC profiles for the consecutive storage- regeneration cycles shown in Figure 5. A clear effect of the barium substitution on NSC is observed: the calcium doped catalyst shows the lowest value, whilst a slight decrease is featured by BTCuO_Sr and, finally, no significant change is detected for BTCuO_Mg. Thus, the NSC of $Ba_{0.9}A_{0.1}Ti_{0.8}Cu_{0.2}O_3$ catalysts decreases as follows: BTCuO ≈ BTCuO_Mg > BTCuO_Sr >> BTCuO_Ca. It is worth mentioning that the NSC for the BTCuO, BTCuO_Sr and BTCuO_Mg catalysts are close to that previously reported in similar experimental conditions for PGM catalysts [37].

The NO_2/NOx ratio was calculated from the NO_2 and NOx concentration at the end of the lean cycle ($time_{cycle}$=300s), and the data corresponding to the 10^{th} cycle are included in Table 4. BTCuO_Mg shows the highest NO_2/NOx ratio, suggesting that it is the most active catalyst for NO to NO_2 oxidation. Even though it seems speculative to consider a direct relationship between NSC and the NO to NO_2 oxidation activity (as the total amount of NO_2 generated cannot be analyzed, just the not adsorbed fraction), the comparison of both values reveal some insights on the effect of the A cation substitution on the catalytic performance. Considering that the most accepted NOx adsorption mechanism on alkaline/alkaline earth oxides [38, 39] involves NO_2 as the main adsorbed compound, the larger amount of NO_2 generated by the magnesium doped perovskite reveals that it has to be the most active catalyst for NO to NO_2 oxidation, as both catalysts (BTCuO and BTCuO_Mg) show similar NSC. This conclusion is supported by the characterization data that show as copper is shifted towards the BTCuO_Mg catalyst surface because magnesium occupies the B-copper-site in the structure (instead of replacing barium in the A site), thus increasing the NO to NO_2

oxidation activity respect to BTCuO, but also keeping the segregation of phases (so, the amount of active sites) and, therefore, allowing a similar NSC. Consequently, the BTCuO_Mg catalyst shows enhanced redox properties which justify its higher activity for NO to NO_2 oxidation, but a similar NSC than BTCuO catalyst as the adsorption sites (due to the presence of segregated phases as Ba_2TiO_4 and $BaCO_3$ [17, 18]) still being present.

Based on this hypothesis, the decrease of the NSC observed for the BTCuO_Sr and BTCuO_Ca catalyst (as they show identical NO_2/NOx ratio) could be correlated with a loss of surface active sites for NOx adsorption. However, only the characterization results obtained for the BTCuO_Ca catalyst support this hypothesis, as the presence of segregated phases (Ba_2TiO_4, $BaCO_3$, etc. considered as plausible NOx adsorption sites) were not observed in XRD pattern. For the BTCuO_Sr catalyst, the presence of segregated phases and the slight shift of copper from the lattice to the surface were observed by XRD, XPS and H_2-TPR and, for hence, the slightly lower NSC of this catalyst cannot be due to a lower amount of NOx adsorption sites. Considering that the substitution of BaO for SrO in a commercial LNT catalyst has no effect on the total NSC of the system [40, 41], a slower reaction pathway could cause the NOx adsorption performance of the BTCuO_Sr catalyst. In order to check this hypothesis, NOx saturation experiments were carried out using a 1 hour lean cycle, and the NSC and NO_2/NOx ratio obtained at the end of the adsorption cycle are also included in Table 4 (NOx saturation). Under these experimental conditions, the BTCuO_Sr catalyst exhibits higher NOx adsorption capacity than BTCuO and BTCuO_Mg catalysts and an identical NO_2 generation ability. Since a longer lean cycle is used, it is assumed that all the catalysts reach the saturation level, thus, it seems that the incorporation of strontium generates the highest amount of active sites for NOx adsorption, but longer time is required to saturate the catalyst surface. Therefore, the performance shown by the BTCuO_Sr catalyst during the NSRC experiments seems to be related to a slower NOx adsorption process.

A deeper study of catalysts after the NSRC and NOx saturation experiments was carried out by ex-situ XRD and XPS, and the results are shown in Figures 6, 7 and 8.

The diffractograms obtained after NOx saturation (Figure 6a) indicate that: i) the perovskite structure remains as the main phase, ii) $Ba(NO_3)_2$ and $BaCO_3$ (formed during the exposure of catalysts to the atmosphere before recording the XRD patterns) are present in all patterns, though the first is hardly noticed for BTCuO_Ca catalyst due its lower NSC iii) Ba_2TiO_4 and CuO phases disappear for the BTCuO, BTCuO_Sr and BTCuO_Mg catalysts, and iv) $Ba_2Ca_2Ti_2O_8$ phase also disappear for BTCuO_Ca catalyst. These data suggest that, at 400ºC and, in the presence of NO/O_2, the Ba_2TiO_4 mixed oxide seems to be one of the NOx adsorbent species forming barium nitrate as a final product:

$$Ba_2TiO_4 + 2NO_2 + \frac{1}{2}O_2 \rightarrow Ba(NO_3)_2 + BaTiO_3$$

In the XRD patterns after the NSRC experiments (shown in Figure 6b) the perovskite structure is also the main phase for all the catalysts suggesting that the structure is not modified. In these patterns, the peaks corresponding to barium nitrate are not identified and, for hence, it can be concluded that the regeneration of the catalyst surface is achieved after every rich cycle. Note that a new diffraction peak, assigned to metallic copper, is observed in all the diffractograms. Considering that the rich cycle (10% H_2/N_2) is the last one before the post-characterization analysis, the presence of this peak could be expected according to H_2-TPR data (Figure 4).

The values of cell parameters and c/a lattice ratio (Figure S2 and Table S2 n Supplementary Information) of the fresh and used catalysts (both in NSRC and NOx saturation experiments) reveal that, after the NOx saturation experiments, the lattice parameters are not significantly changed respect to fresh catalysts and, consequently, it is confirmed that the structure is not modified. Additionally, as peaks corresponding to copper species were not identified in XRD patterns after the NOx saturation, it can be concluded that copper remains incorporated into the structure. However, after the NSRC experiments, the c/a ratio decreases to a value close to that obtained for the bare $BaTiO_3$ perovskite for BTCuO and BTCuO_Ca catalysts, indicating a structure distortion during the reduction cycle. As reduced copper is identified in the XRD patterns recorded after NSRC experiments, the change of the lattice parameters has to be due to the segregation

of copper to the perovskite surface as a consequence of its reduction during the regeneration cycle. Thus, it seems that copper is able to shift towards the surface under reducing conditions and, to come back into the lattice under oxidizing conditions, without a collapse of the perovskite structure. For the BTCuO_Sr and BTCuO_Mg catalysts, the presence of metallic copper in the XRD patterns after the NSRC experiments suggests that copper also changes its position after NOx storage cycles, but, in this case, the perovskite structure is not modified. For these two perovskites, strontium and magnesium are inserted into the perovskite structure causing a distortion that is hold during the exposure to reducing conditions since strontium and magnesium are not reduced and, therefore, they still being inserted into the perovskite structure. Thus, the incorporation of strontium and magnesium into the perovskite improves its structure stability. This is in agreement with the results obtained by Nishihata et al [42], who proved that the shift of palladium into and out of the $LaFe_{0.57}Co_{0.38}Pd_{0.05}O_3$ perovskite structure (depending on the atmosphere conditions) lead to a self-regenerating catalyst with enhanced stability to long-term use and ageing.

The deconvolution of the XPS spectra of the $Cu2p_{3/2}$ transition after NOx saturation experiments (Figure 7) shows, as for the fresh catalysts, two contributions (at ≈ 933 eV and ≈ 935 eV) and a "shake-up" peak (942 eV) corresponding to the presence of Cu (II). This fact points out that the copper environment is not modified after NOx storage. On the contrary, the analysis of the XPS Cu spectra after NSRC experiments reveals the presence of reduced copper since the main XPS peak appears below 933 eV and the "shake-up" peak at 942 eV almost vanishes for all the catalysts. The Cu/(Ba + A + Ti + Cu) post-reaction ratios calculated for the used catalysts (Table S1 in Supporting Information) reveal an increase after both experiments, but, the values obtained for the NOx saturated samples are closer to the nominal ones (0.1) supporting that copper is into the structure. However, after the NSRC experiment, the Cu/(Ba + A + Ti + Cu) XPS ratio increases considerably indicating a higher concentration of copper (as reduced copper) on the catalysts surface due to the migration from the lattice to the surface. Thus, these data support the conclusion drawn from XRD about the change of the copper position in the structure depending on the atmosphere conditions.

In Figure 8 the XPS spectra obtained for the O1s transition of the used samples are shown. Compared to fresh catalysts, except for BTCuO_Ca catalyst, an increase in the intensity of the 533 eV peak for NOx saturated samples can be noticed. This peak (based on the identification of the N1s peak at 407 eV for all the catalysts [43] (not shown)) corresponds to nitrates adsorbed species that was also observed by XRD. After the NSRC experiments, the peak corresponding to carbonate groups becomes more intense, because the decomposition of barium nitrates during the regeneration yields BaO, which is identified as barium carbonate by XPS (due to CO_2 adsorption from the atmosphere). Furthermore, the absence of N1s transition peaks (ascribed to nitrogen surface groups) after NSRC experiments, supports the total regeneration of the catalysts surface.

3.2.2. SO_2 tolerance experiments.

Figure 9 shows the NSC profiles at 400ºC for the NSRC experiments carried out using a $NO/SO_2/O_2$ atmosphere during the lean cycle. It is clearly observed that when SO_2 is also fed into the reactor, the partial substitution of barium has a positive effect on the catalyst performance as, for the first lean cycle, all the substituted catalysts are more active than BTCuO. Note that, in the presence of SO_2, the NSC of the BTCuO catalyst is drastically inhibited from the first lean cycle, whereas for all the substituted catalysts the NSC progressively decreases along the cycles until an unacceptably low value is reached after the 6^{th} cycle. As it is widely reported, the regeneration of the catalysts surface during the rich cycle is not achieved because a higher regeneration temperature is needed for the removal of the sulfates formed in the presence of SO_2 [44]. Therefore, it seems that the addition of strontium, calcium and magnesium improves the tolerance to SO_2, being BTCuO_Sr and BTCuO_Mg the most resistant catalysts.

The NO_2/NOx ratio at the end of the 10^{th} lean cycle, in the presence of sulfur dioxide, is 4% for all the catalysts. Thus, it seems that the actives sites for NO to NO_2 oxidation are also being poisoned by SO_2.

Ex-situ XRD and Diffuse Reflectance Infrared Fourier Transform Spectroscopy (DRIFTS) were used to identify nitrogen and sulfur species formed on the catalysts

surface after NOx saturation experiments in the presence of SO_2. XRD patterns (Figure S3 in Supplementary Information) show that all catalysts present: i) the main peaks corresponding to $BaTiO_3$ perovskite structure, ii) the absence of the peak corresponding to the Ba_2TiO_4 phase, and iii) the absence of barium nitrates or barium sulfates peaks. These peaks cannot be clearly distinguished from the noise of the diffractograms due to the low amount of NOx adsorbed in the presence of SO_2 and, presumably, to the formation of surface or bulk amorphous sulfates, respectively. Figure 10 shows the DRIFTS spectra recorded after the NOx saturation experiments in the presence of SO_2, where the following peaks are observed: i) at 1384 and 1774 cm^{-1} (blue line), that are ascribed to bulk barium nitrate groups [45,46], and confirming that NOx is adsorbed on the catalysts surface even in the presence of SO_2, and ii) from 950 to 1250 cm^{-1} (red lines), a group of broad and not well defined peaks that, tentatively, can be ascribed to bulk sulfates (984, 1080, 1120 and 1184 cm^{-1}) and surface sulfates (1060, 1140 and 1217 cm^{-1}) [47]. Comparing the intensities of the nitrate bands, it seems that the BTCuO_Ca catalyst shows the lowest NOx coverage, and that the BTCuO_Sr catalyst shows the highest SO_2 coverage. Nevertheless, it is worth mentioning that a quantitative analysis of the catalysts coverage by using the intensity of the DRIFTS signals can be fairly speculative as the IR absorption cross-section of the adsorbed species can be significantly affected by adsorption configuration [48,49].

In summary, it is concluded that the presence of SO_2 leads to the loss of NSC for all the catalysts (more pronounced for BTCuO) due to the adsorption of SO_2 on perovskite surface which blocks the NO to NO_2 oxidation and the NOx adsorption sites.

3.2.3. SO_2 regeneration experiments.

The presence of SO_2 in the gas stream has a poisoning effect on the catalysts performance which cannot be reverted during the rich cycle and, consequently, the deactivation of the catalysts is observed. However, it is interesting to determine if the NSC can be restored by SO_2 removing. Thus Figure 11 shows the NSC profiles obtained following the procedure detailed in the experimental section.

The results of the first and second sections of these profiles have been previously discussed: i) the first 5 cycles correspond to the catalysts performance in NSRC experiments, previously shown in Figure 5 and, ii) the following 5 cycles are those obtained in the presence of sulfur dioxide correspond to the profiles appear in Figure 9. So, the new results are featured, only, in the third part of the experiment. A fast recovery of the NSC is observed for BTCuO, BTCuO_Sr and BTCuO_Mg catalysts during the three first adsorption-regeneration cycles. Afterwards, the NSC shows a more slowly increase until: i) the total regeneration is achieved for BTCuO_Sr and BTCuO_Mg, for which a final NSC slightly higher than the corresponding to the fresh catalysts is observed, ii) BTCuO shows a lower NSC and iii) BTCuO_Ca is not regenerated at all.

The NO_2/NOx ratio profiles obtained during the whole experiments (Figure S4 in Supplementary Information) confirmed the loss of NO oxidation activity in the presence of SO_2 for all the catalysts, as the NO_2/NOx ratio is as low as 4% from the very first cycle. This result justifies the loss of NSC during the second set of 5 cycles. Once SO_2 feeding stops, the NO_2/NOx ratio increases for all the catalysts, recovering the NO_2 generation capacity after the 4^{th} storage-regeneration cycle. An unexpected increase in the amount of NO_2 released after catalysts regeneration is observed for all the mixed oxides and, considering that only the NO_2 that is not adsorbed can be registered, this fact suggests that the NOx adsorption sites seem not to be totally regenerated.

Thus, based on the NSC results, it seems that a significant fast regeneration of the BTCuO, BTCuO_Sr and BTCuO_Mg catalysts is achieved by just removing SO_2 from the gas stream. This means that the cleaning of the perovskites surface takes place because NO/NO_2 molecules are able to quickly shift SO_2 from the NO oxidation and NOx adsorption sites [7,47]. It has to be highlighted that the regeneration of the BTCuO_Sr and BTCuO_Mg catalysts seems to be faster and more effective than for BTCuO, because BTCuO_Sr and, especially, BTCuO_Mg catalyst, are able to recover the oxidation sites, thus, generating a larger amount of NO_2 will is able to quick shift SO_2 from the NOx adsorption sites.

XRD patterns after SO_2 regeneration experiments (Figure S5 in Supplementary Information), confirm the high stability of the catalysts as, even after SO_2 exposure and regeneration, the perovskite structure is preserved. The XRD patterns after the SO_2 regeneration experiments are identical to those recorded after NSRC experiments (Figure 6), as peaks for nitrates and sulfates are not identified and, as additional phases, only the peaks ascribed to $BaCO_3$ and metallic copper (coming from the nitrate groups regeneration and the reduction of lattice copper, respectively) are noticed. A modification of the c/a lattice ratio is observed for the BTCuO and BTCuO_Ca catalysts (Figure S6 in Supplementary Information) indicating a distortion of the structure due to the shift of the reduced copper towards the perovskite surface during the rich cycle (reducing conditions). On the contrary, the c/a lattice ratio is not modified for BTCuO_Sr and BTCuO_Mg catalysts due to the high stability of the structure during the rich cycle. It is worth mentioning that the most regenerable catalysts (BTCuO_Sr and BTCuO_Mg) are those presenting the most stable structure which assures that both, NO oxidation and NOx adsorption sites, are not modified during cyclic experimental conditions.

The presence of reduced copper is confirmed by the XPS spectra of the $Cu2p_{3/2}$ transition after SO_2 regeneration (Figure S7 in Supplementary Information) as the main XPS peak appears below 933 eV and, it is also observed a decrease of the "shake-up" peak intensity at 942 eV, compared to the as-prepared samples. However, for the BTCuO_Sr and BTCuO_Mg catalysts, the presence of reduced copper is less evident, in agreement with the lower catalysts reducibility observed during H_2-TPR experiments (Figure 5). The XPS Cu/(Ba + A + Ti + Cu) post-reaction ratios (Table S1 in Supplementary Information) confirm that the fraction of copper on the catalysts surface increases due to the migration from the lattice to the surface. Additionally, the XPS spectra obtained for the O1s transition after SO_2 regeneration (Figure S7 in Supplementary Information) point out an increase in the intensity of the peak assigned to carbonate. As indicated before, this is due to the decomposition of the barium nitrate generates BaO which is next carbonated by contact with the atmospheric CO_2. The analysis of the N1s transition indicates the absence of peaks ascribed to nitrogen surface

groups after SO_2 regeneration experiments, supporting the total regeneration of the catalysts surface.

The DRIFTS spectra recorded after the SO_2 regeneration experiments are shown in Figure 12. Firstly, peaks assigned to bulk barium nitrates at 1384 and 1774 cm^{-1} are not observed, confirming that the NOx adsorbed is removed from the catalysts surface during rich cycle. Secondly, from 950 to 1250 cm^{-1}, peaks corresponding to sulfate species (red lines) can be clearly identified indicating that the total regeneration of catalysts is not achieved. The comparison of these spectra with those obtained after the SO_2 tolerance experiments (Figure 10) evidences the presence of IR bands corresponding only to bulk barium sulfates, since more defined peaks centered at 984, 1080, 1120 and 1184 cm^{-1} are identified. This result indicates that only the surface sulfates are being removed during the regeneration step.

In summary, from catalytic activity and post-reaction characterization results, it can be concluded that: i) the NSC is recovered after SO_2 removing from the gas stream for all the $Ba_{0.9}A_{0.1}Ti_{0.8}Cu_{0.2}O_3$ catalysts, except for BTCuO_Ca, ii) the perovskite structure is preserved and iii) the total regeneration of the catalysts surface is not achieved due to the presence of bulk sulfates block the NO oxidation and NOx adsorption sites on the catalysts surface. This effect is more evident for BTCuO_Ca, which is the catalyst with the lowest amount of adsorption sites, but also in a lower extent for BTCuO catalyst. The BTCuO_Sr and BTCuO_Mg catalysts do not lose the NSC after SO_2 regeneration because; i) the amount of bulk sulfates formed seems to be lower than for BTCuO_Ca and BTCuO catalysts and ii) these catalysts show a faster recovery of the NO to NO_2 oxidation activity and, consequently, of the NSC.

4. CONCLUSIONS.

Based on the results obtained, it can be concluded that SO_2 inhibits both NO oxidation and NOx adsorption sites on the catalysts surface, but, a promoting effect on the tolerance and regeneration versus SO_2 is observed for strontium and magnesium.

In the BTCuO_Sr catalyst, due to the substitution of Ba (II) by Sr (II) in the A site, the amount of the NOx adsorption active sites is larger than in the bare catalyst

(BTCuO) and, consequently, this catalyst shows the highest NSC in the long-term adsorption (NOx saturation) experiments. Therefore, even though some of these sites would remain blocked by the bulk sulfates, this does not involve a significant decrease of the NSC after SO_2 regeneration. In BTCuO_Mg catalyst, Mg (II) replaces Cu (II) in the B site (instead of Ba (II) in the A site or Ti (IV) in B site) causing a shift of the Cu (II) towards the catalyst surface, which improves the NO to NO_2 oxidation activity. Thus, as new adsorption sites are not generated, BTCuO_Mg catalyst shows a NSC similar to that of the BTCuO catalyst. On the other hand, BTCuO_Sr and BTCuO_Mg catalysts present the most stable perovskite (pseudo-cubic) structure which is not significantly modified during reduction cycles, thus preserving the amount of surface actives sites during NOx storage cycles.

The addition of calcium does not involve the segregation of potential active phases (as Ba_2TiO_4 and $BaCO_3$), and for hence, the amount of NOx adsorption sites is lower than for BTCuO, thus, showing the lowest NSC. Additionally, it is not possible to regenerate the NSC of the BTCuO_Ca catalyst after SO_2 exposure since SO_2 remains adsorbed on the catalyst surface forming bulk sulfates which block the NOx adsorption sites.

5. ACKNOWLEDGMENTS.

The authors thank Spanish Government (MINECO) and UE (FEDER Founding) (project CTQ2015-64801-R) and Generalitat Valenciana (project PROMETEO II/2018/076) for the financial support. V. Albaladejo-Fuentes thanks the University of Alicante for his Ph.D. grant.

6. REFERENCES.

[1] A.O. Hasan, A. Abu-jrai, D. Turner, A. Tsolakis, H.M. Xu, S.E. Golunski, J.M. Herreros, Atmos. Environ. 129 (2016) 210–217.

[2] S. Polat, A. Uyumaz, H. Solmaz, E. Yilmaz, T. Topgül, H.S. Yücesu, Int. J. Green Energy 13 (2016) 63–70.

[3] W. Epling, I. Nova, J. Szanyi, A. Yezerets, Catal. Today 151 (2010) 201.

[4] J.P. Breen, M. Marella, C. Pistarino, J.R.H. Ross, Catal. Letters 80 (2002) 123–128.

[5] L.J. Gill, P.G. Blakeman, M. V Twigg, A.P. Walker, Top. Catal. 28 (2004) 157–164.

[6] P. Forzatti, L. Lietti, I. Nova, E. Tronconi, Catal. Today 151 (2010) 202–211.

[7] W.S. Epling, L.E. Campbell, A. Yezerets, N.W. Currier, J.E. Parks, Catal. Rev. Sci. Eng. 46 (2004) 163–245.

[8] M. Bowker, Chem. Soc. Rev. 37 (2008) 2204–2211.

[9] T.J. Toops, B.G. Bunting, K. Nguyen, A. Gopinath, Catal. Today 123 (2007) 285–292.

[10] Y. Liu, M. Meng, X.G. Li, L.H. Guo, Y.Q. Zha, Chem. Eng. Res. Des. 86 (2008) 932–940.

[11] G. Qi, W. Li, Catal. Today 184 (2012) 72–77.

[12] S. Royer, D. Duprez, F. Can, X. Courtois, C. Batiot-Dupeyrat, S. Laassiri, H. Alamdari, Chem. Rev. 114 (2014) 10292–10368.

[13] X. Li, C. Chen, C. Liu, H. Xian, L. Guo, J. Lv, Z. Jiang, P. Vernoux, ACS Catal. 3 (2013) 1071–1075.

[14] C.H. Kim, G. Qi, K. Dahlberg, W. Li, Science (80-.). 327 (2010) 1624–1627.

[15] W. Shen, A. Nitta, Z. Chen, T. Eda, A. Yoshida, S. Naito, J. Catal. 280 (2011) 161–167.

[16] L. Righini, F. Gao, L. Lietti, J. Szanyi, C.H.F. Peden, Appl. Catal. B Environ. 181 (2016) 862–873.

[17] V. Albaladejo-Fuentes, F.E. López-Suárez, M.S. Sánchez-Adsuar, M.J. Illán-Gómez, Appl. Catal. A Gen. 488 (2014) 189–199.

[18] V. Albaladejo-Fuentes, F.E. López-Suárez, M.S. Sánchez-Adsuar, M.J. Illán-Gómez, Appl. Catal. A Gen. 519 (2016) 7–15.

[19] T.J. Toops, N.A. Ottinger, C. Liang, J.A. Pihl, E.A. Payzant, Catal. Today 160 (2011) 131–136.

[20] S. Fang, L. Wang, Z. Sun, N. Feng, C. Shen, P. Lin, H. Wan, G. Guan, Catal. Commun. 49 (2014) 15–19.

[21] G. Saracco, F. Geobaldo, G. Baldi, Appl. Catal. B Environ. 20 (1999) 277–288.

[22] M.A. Peña, J.L.G. Fierro, Chem. Rev. 101 (2001) 1981–2017.

[23] S. Matsumoto, Y. Ikeda, H. Suzuki, M. Ogai, N. Miyoshi, Appl. Catal. B Environ. 25 (2000) 115–124.

[24] T. Kobayashi, T. Yamada, K. Kayano, (1997).

[25] J.S. Hepburn, E. Thanasiu, D.A. Dobson, W.L. Watkins, (1996).

[26] H. Zhang, G. Chen, Y. Li, Y. Teng, Int. J. Hydrogen Energy 35 (2010) 2713–2716.

[27] Y.B. Khollam, S.B. Deshpande, H.S. Potdar, S.V. Bhoraskar, S.R. Sainkar, S.K. Date, Mater. Charact. 54 (2005) 63–74.

[28] M.C. Gust, L.A. Momoda, N.D. Evans, M.L. Mecartney, J. Am. Ceram. Soc. 84 (2001) 1087–1092.

[29] M.M. Rashad, A.O. Turky, A.T. Kandil, J. Mater. Sci. Mater. Electron. 24 (2013) 3284–3291.

[30] D. Fu, M. Itoh, S. Koshihara, J. Phys. Condens. Matter 22 (2010) 052204.

[31] S. Xu, Y. Qu, C. Zhang, J. Appl. Phys. 106 (2009) 014107.

[32] B. Su, T.W. Button, J. Appl. Phys. 95 (2004) 1382–1385.

[33] H. Miao, M. Dong, G. Tan, Y. Pu, J. Electroceramics 16 (2006) 297–300.

[34] J. Ghijsen, L.H. Tjeng, J. Van Elp, H. Eskes, J. Westerink, G.A. Sawatzky, M.T. Czyzyk, Phys. Rev. B 38 (1988) 11322–11330.

[35] N.A. Merino, B.P. Barbero, P. Eloy, L.E. Cadús, Appl. Surf. Sci. 253 (2006) 1489–1493.

[36] H. He, H.. Dai, C.. Au, Appl. Catal. B Environ. 33 (2001) 65–80.

[37] K.S. Kabin, R.L. Muncrief, M.P. Harold, Catal. Today 96 (2004) 79–89.

[38] I. Nova, L. Castoldi, L. Lietti, E. Tronconi, P. Forzatti, F. Prinetto, G. Ghiotti, J. Catal. 222 (2004) 377–388.

[39] E. Fridell, H. Persson, L. Olsson, M. Skoglundh, Catal. Letters 66 (2000) 71–74.

[40] J. Dawody, I. Tönnies, E. Fridell, M. Skoglundh, Top. Catal. 42–43 (2007) 183–187.

[41] P.-H. Han, Y.-K. Lee, S.-M. Han, H.-K. Rhee, Top. Catal. 16/17 (2001) 165–170.

[42] Y. Nishihata, J. Mizuki, H. Tanaka, M. Uenishi, M. Kimura, J. Phys. Chem. Solids 66 (2005) 274–282.

[43] P.J. Schmitz, R.J. Baird, J. Phys. Chem. B 106 (2002) 4172–4180.

[44] J. Dawody, M. Skoglundh, L. Olsson, E. Fridell, 234 (2005) 206–218.

[45] E. Roedel, A. Urakawa, S. Kureti, A. Baiker, Phys. Chem. Chem. Phys. 10 (2008) 6190–8.

[46] K.I. Hadjiivanov, Catal. Rev. Sci. Eng. 42 (2000) 71–144.

[47] G.S. Şentürk, E.I. Vovk, V.I. Zaikovskii, Z. Say, A.M. Soylu, V.I. Bukhtiyarov, E. Ozensoy, Catal. Today 184 (2012) 54–71.

[48] F. Zaera, Chem. Soc. Rev. 43 (2014) 7624–7663.

[49] J. Sirita, S. Phanichphant, F.C. Meunier, Anal. Chem. 79 (2007) 3912–3918.

Table.1 Experimental conditions for the SO_2 regeneration tests.

Catalytic test	Cycles	Lean cycle conditions	Rich cycle conditions
NOx adsorption	5	500 ppm NO, 5% O_2, N_2 / 5 min.	10% H_2, N_2 / 3 min.
SO_2 tolerance	5	500 ppm NO, 100 ppm SO_2, 5% O_2, N_2 / 5 min.	10% H_2, N_2 / 3 min.
SO_2 regenerability	10	500 ppm NO, 5% O_2, N_2 / 5 min.	10% H_2, N_2 / 3 min.

Table 2. Nomenclature, ICP-OES metal content and specific surface area of the $Ba_{0.9}A_{0.1}Ti_{0.8}Cu_{0.2}O_3$ catalysts.

Catalysts formula	Nomenclature	Nominal A (wt%)	ICP-OES A (wt%)	Nominal Cu (wt%)	ICP-OES Cu (wt%)	S_{BET} (m^2/g)
$BaTiO_3$	BTO	-	-	-	-	9
$BaTi_{0.8}Cu_{0.2}O_3$	BTCuO	-	-	5.4	5.4	21
$Ba_{0.9}Sr_{0.1}Ti_{0.8}Cu_{0.2}O_3$	BTCuO_Sr	3.8	3.7	5.5	5.5	12
$Ba_{0.9}Ca_{0.1}Ti_{0.8}Cu_{0.2}O_3$	BTCuO_Ca	1.8	1.7	5.6	5.7	4
$Ba_{0.9}Mg_{0.1}Ti_{0.8}Cu_{0.2}O_3$	BTCuO_Mg	1.1	1.0	5.6	5.5	4

Table 3. XRD, XPS and H_2-TPR characterization data of the $Ba_{0.9}A_{0.1}Ti_{0.8}Cu_{0.2}O_3$ catalysts.

Catalyst	a (Å)*	c (Å)*	FWHM (2 0 0) / FWHM (1 1 1)	Cu/ Ba+A+Ti+Cu (XPS)	O_L/ Ba+A+Ti+Cu (XPS)	% Cu reduced
BTO	4,007	4,003	1.76	-	1.78	-
BTCuO	4,005	4,005	1.66	0.06	1.44	95
BTCuO_Sr	3,986	3,986	1.21	0.08	0.98	86
BTCuO_Ca	4,007	4,004	2.11	0.06	1.08	94
BTCuO_Mg	4,009	4,011	1.05	0.08	1.09	94

** Lattice parameters calculated from XRD data.*

Table 4. NSC and NO_2/NOx ratio of the $Ba_{0.9}A_{0.1}Ti_{0.8}Cu_{0.2}O_3$ catalysts during NSRC and saturation experiments under NO/O_2 atmosphere at 400ºC.

Catalyst	NSRC experiments[a)]		NOx saturation experiments[b)]	
	NSC (µmol/g.cat.)	NO_2/NO_x (%)	NSC (µmol/g.cat.)	NO_2/NO_x (%)
BTCuO	298	16	412	22
BTCuO_Sr	240	15	460	22
BTCuO_Ca	139	16	313	17
BTCuO_Mg	296	20	415	22

a) Experiment conditions: i) 500 ppm NO + 5% O_2 balanced with N_2 for the lean cycle (5 min) and ii) 10% H_2 in N_2 balance for the rich cycle (3 min), temperature set at 400ºC.

b) Experiment conditions: i) 500 ppm NO + 5% O_2 balanced with N_2, temperature set at 400ºC for 1h.

Figure 1. a) XRD patterns of the $Ba_{0.9}A_{0.1}Ti_{0.8}Cu_{0.2}O_3$ catalysts and b) magnification of the 2Θ diffraction angle area corresponding to the $BaTiO_3$ perovskite main diffraction peak.

Figure 2. XPS spectra of the a) $Cu2p^{3/2}$ transition and b) O1s transition for the bare $Ba_{0.9}A_{0.1}Ti_{0.8}Cu_{0.2}O_3$ catalysts.

Figure 3. O_2-TPD profiles of the $Ba_{0.9}A_{0.1}Ti_{0.8}Cu_{0.2}O_3$ catalysts.

Figure 4. H_2-TPR profiles of the $Ba_{0.9}A_{0.1}Ti_{0.8}Cu_{0.2}O_3$ catalysts.

Figure 5. NSC of the $Ba_{0.9}A_{0.1}Ti_{0.8}Cu_{0.2}O_3$ catalysts during NSRC at 400ºC. (Experiments were carried out under a gas flow of 500 ml/min containing: i) 500 ppm NO + 5% O_2 balanced with N_2 for the lean cycle (5 min) and ii) 10% H_2 in N_2 balance for the rich cycle (3 min)).

Figure 6. XRD patterns of the $Ba_{0.9}A_{0.1}Ti_{0.8}Cu_{0.2}O_3$ catalysts: a) after NOx saturation experiment (Experiment conditions: gas flow of 500 ml/min containing 500 ppm NOx, 5 % O_2 in N_2 balance, 400ºC for 1h) and b) after NSRC experiments (Experiment conditions: i) 500 ppm NO + 5% O_2 balanced with N_2 for the lean cycle (5 min) and ii) 10% H_2 in N_2 balance for the rich cycle (3 min), temperature set at 400ºC).

Figure 7. XPS spectra of the $Cu2p^{3/2}$ transition for the $Ba_{0.9}A_{0.1}Ti_{0.8}Cu_{0.2}O_3$ catalysts after NSRC (Experiment conditions: i) 500 ppm NO + 5% O_2 balanced with N_2 for the lean cycle (5 min) and ii) 10% H_2 in N_2 balance for the rich cycle (3 min), temperature set at 400ºC) and NOx saturation experiments (Experiment conditions: gas flow of 500 ml/min containing 500 ppm NOx, 5 % O_2 in N_2 balance, 400ºC for 1h).

Figure 8. XPS spectra of the O1s transition for the $Ba_{0.9}A_{0.1}Ti_{0.8}Cu_{0.2}O_3$ catalysts after NSRC (Experiment conditions: i) 500 ppm NO + 5% O_2 balanced with N_2 for the lean cycle (5 min) and ii) 10% H_2 in N_2 balance for the rich cycle (3 min), temperature set at 400ºC) and NOx saturation experiments (Experiment conditions: gas flow of 500 ml/min containing 500 ppm NOx, 5 % O_2 in N_2 balance, 400ºC for 1h).

Figure 9. NSC of the $Ba_{0.9}A_{0.1}Ti_{0.8}Cu_{0.2}O_3$ catalysts during NSRC experiments under $NO/SO_2/O_2$ atmosphere at 400ºC (Experiment conditions: i) 500 ppm NO + 100 ppm SO_2 + 5% O_2 balanced with N_2 for the lean cycle (5 min) and ii) 10% H_2 in N_2 balance for the rich cycle (3 min), temperature set at 400ºC).

Figure 10. DRIFT spectra recorded for the $Ba_{0.9}A_{0.1}Ti_{0.8}Cu_{0.2}O_3$ catalysts after 1hour of lean cycle with SO_2 presence. (Experiment conditions: i) 500 ppm NO + 100 ppm SO_2 + 5% O_2 balanced with N_2, 400ºC for 1h). Most relevant peaks are indicated as: Barium nitrates (blue line) and barium sulfates (red line).

Figure 11. NSC of the $Ba_{0.9}A_{0.1}Ti_{0.8}Cu_{0.2}O_3$ catalysts during SO_2 regeneration experiments at 400ºC (Experiment conditions: i) 500 ppm NO + 5% O_2 balanced with N_2 or 500 ppm NO + 100 ppm SO_2 + 5% O_2 balanced with N_2 for the lean cycle (5 min) and ii) 10% H_2 in N_2 balance for the rich cycle (3 min), temperature set at 400ºC).

Figure 12. DRIFT spectra recorded for the $Ba_{0.9}A_{0.1}Ti_{0.8}Cu_{0.2}O_3$ catalysts after SO_2 regeneration experiments (Experiment conditions: i) 500 ppm NO + 5% O_2 balanced with N_2 or 500 ppm NO + 100 ppm SO_2 + 5% O_2 balanced with N_2 for the lean cycle (5 min) and ii) 10% H_2 in N_2 balance for the rich cycle (3 min), temperature set at 400ºC). Barium sulfates peaks positions are indicated with red lines.

Figure.1

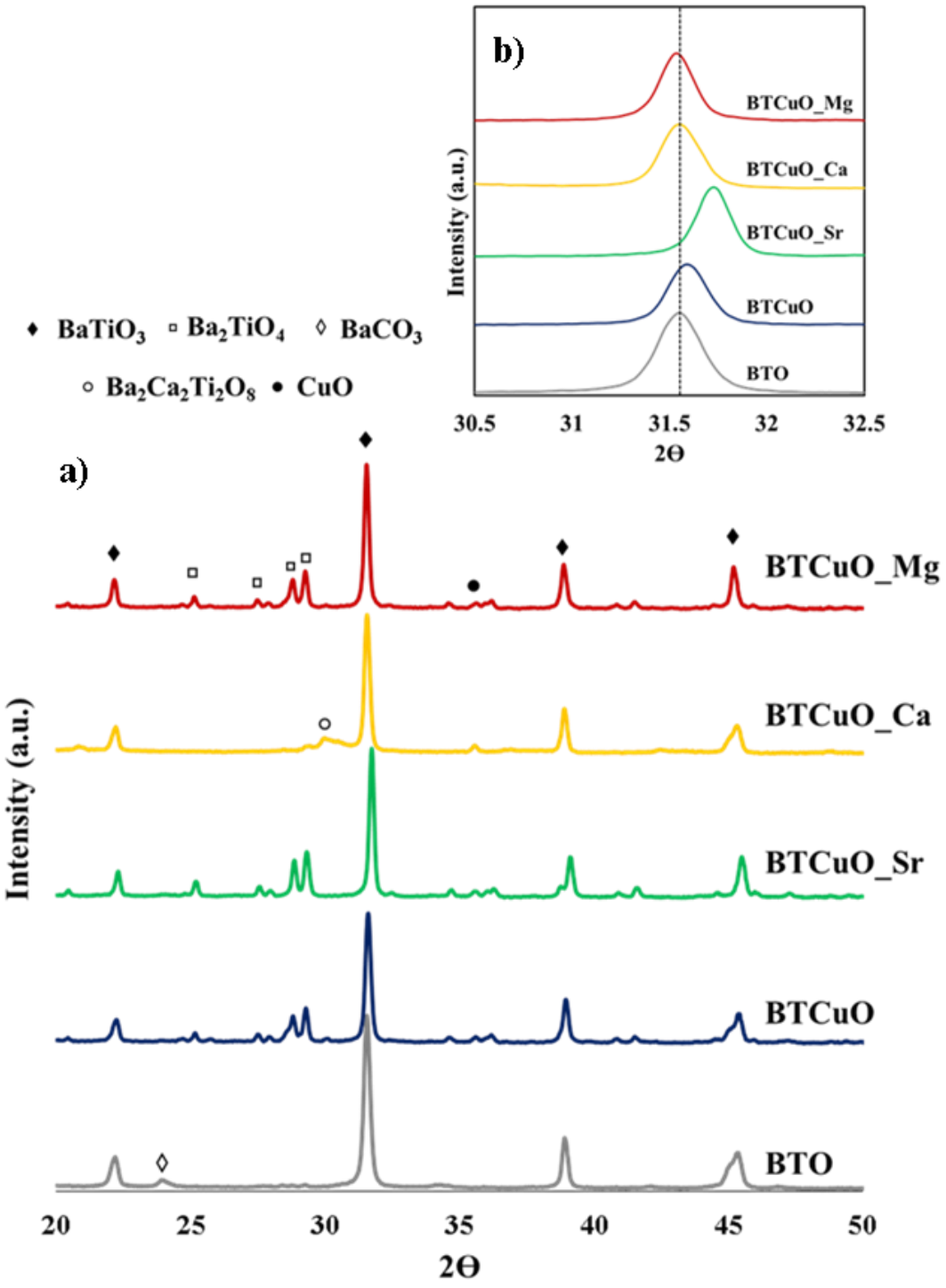
b)
BTCuO_Mg
BTCuO_Ca
BTCuO_Sr
BTCuO
BTO
Intensity (a.u.)
30.5
31
31.5
32
32.5
2Θ
♦ BaTiO3 ▫ Ba2TiO4 ◊ BaCO3
○ Ba2Ca2Ti2O8 • CuO
a)
BTCuO_Mg
BTCuO_Ca
BTCuO_Sr
BTCuO
BTO
Intensity (a.u.)
20
25
30
35
40
45
50
2Θ

Figure 2.

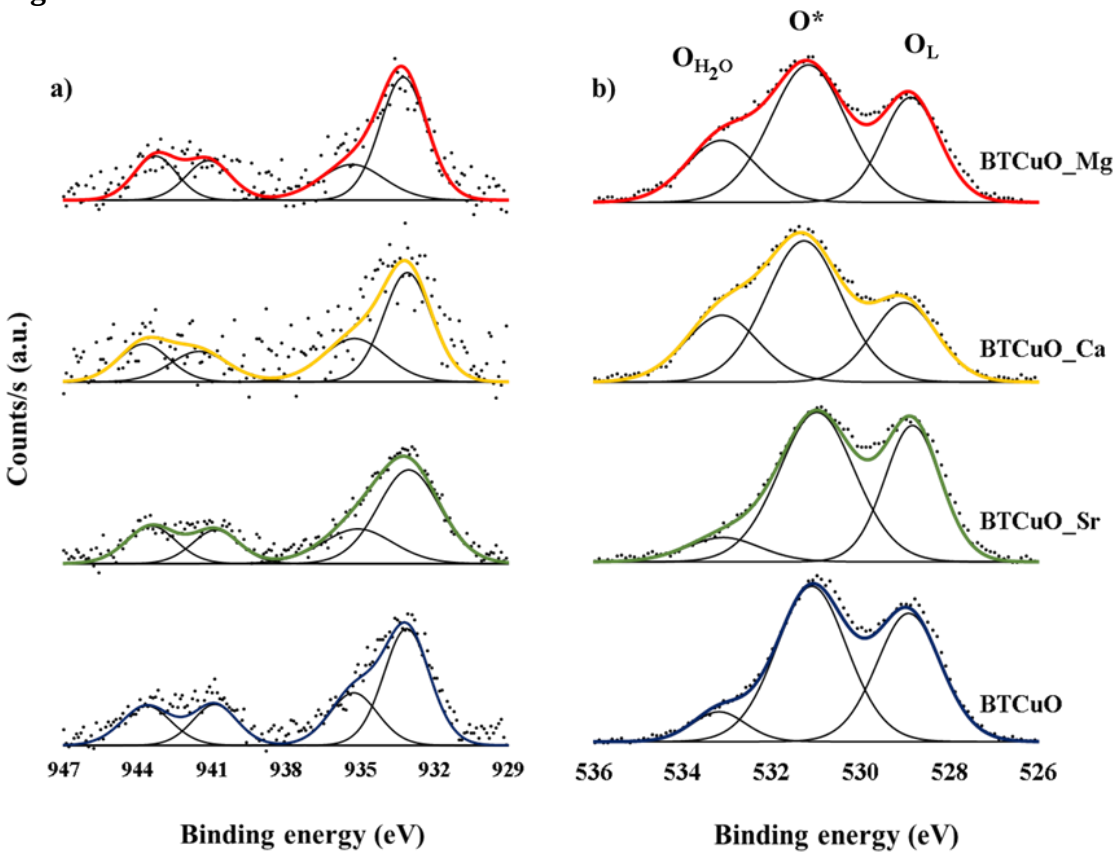
a)
b)
O*
O_{H_2O}
O_L
BTCuO_Mg
BTCuO_Ca
BTCuO_Sr
BTCuO
Counts/s (a.u.)
947
944
941
938
935
932
929
536
534
532
530
528
526
Binding energy (eV)
Binding energy (eV)

Figure 3.

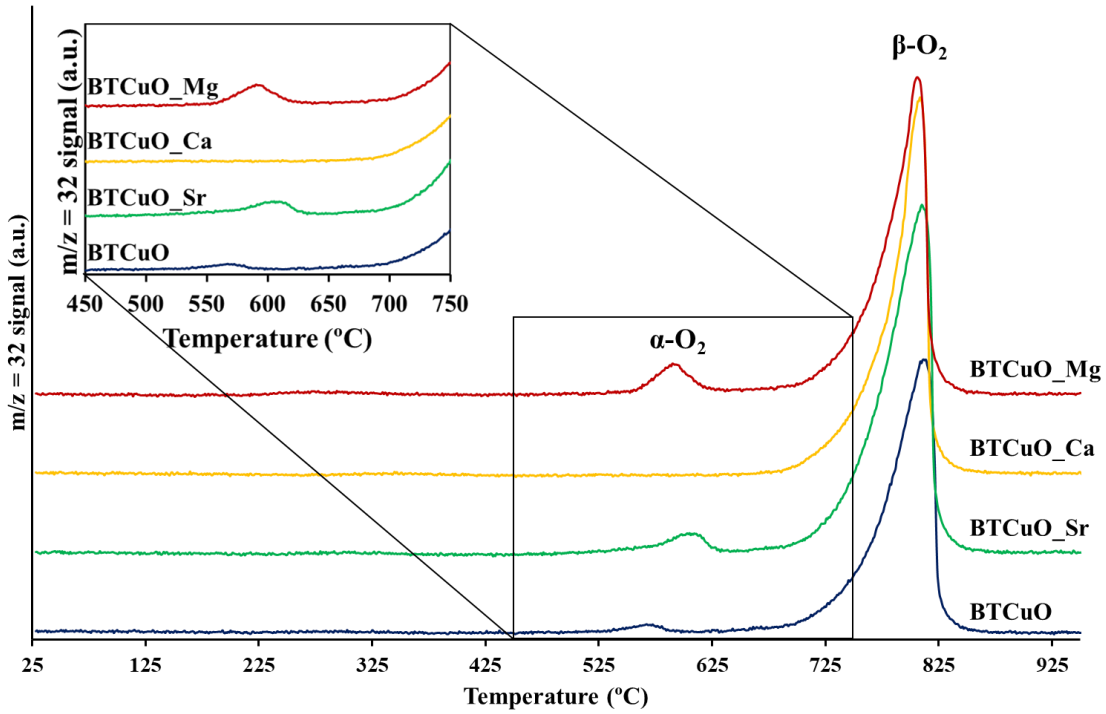
m/z = 32 signal (a.u.)
BTCuO_Mg
BTCuO_Ca
BTCuO_Sr
BTCuO
450 500 550 600 650 700 750
Temperature (°C)
β-O2
α-O2
BTCuO_Mg
BTCuO_Ca
BTCuO_Sr
BTCuO
25 125 225 325 425 525 625 725 825 925
Temperature (°C)

Figure 4.

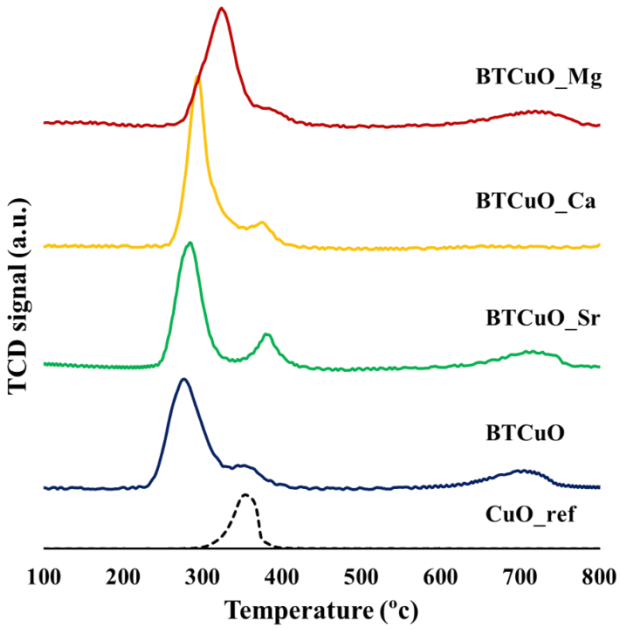
BTCuO_Mg
BTCuO_Ca
BTCuO_Sr
BTCuO
CuO_ref
TCD signal (a.u.)
100
200
300
400
500
600
700
800
Temperature (°c)

Figure 5.

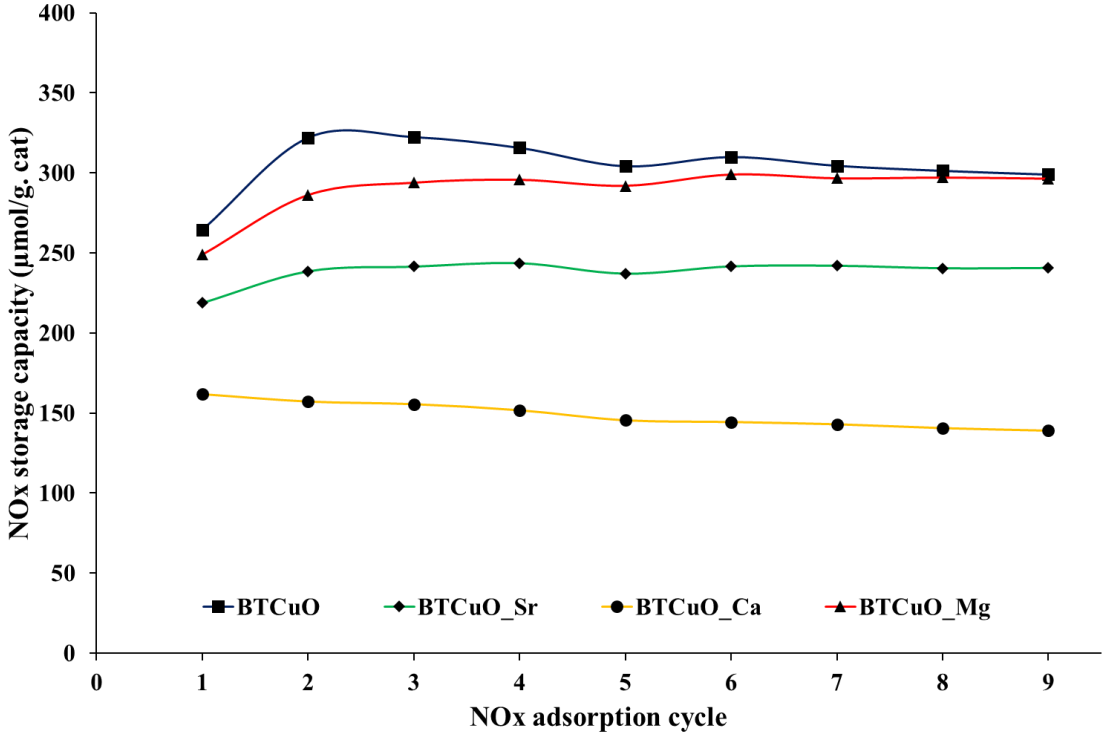
400
350
300
250
200
150
100
50
0
NOx storage capacity (µmol/g. cat)
0
1
2
3
4
5
6
7
8
9
NOx adsorption cycle
BTCuO
BTCuO_Sr
BTCuO_Ca
BTCuO_Mg

Figure 6.

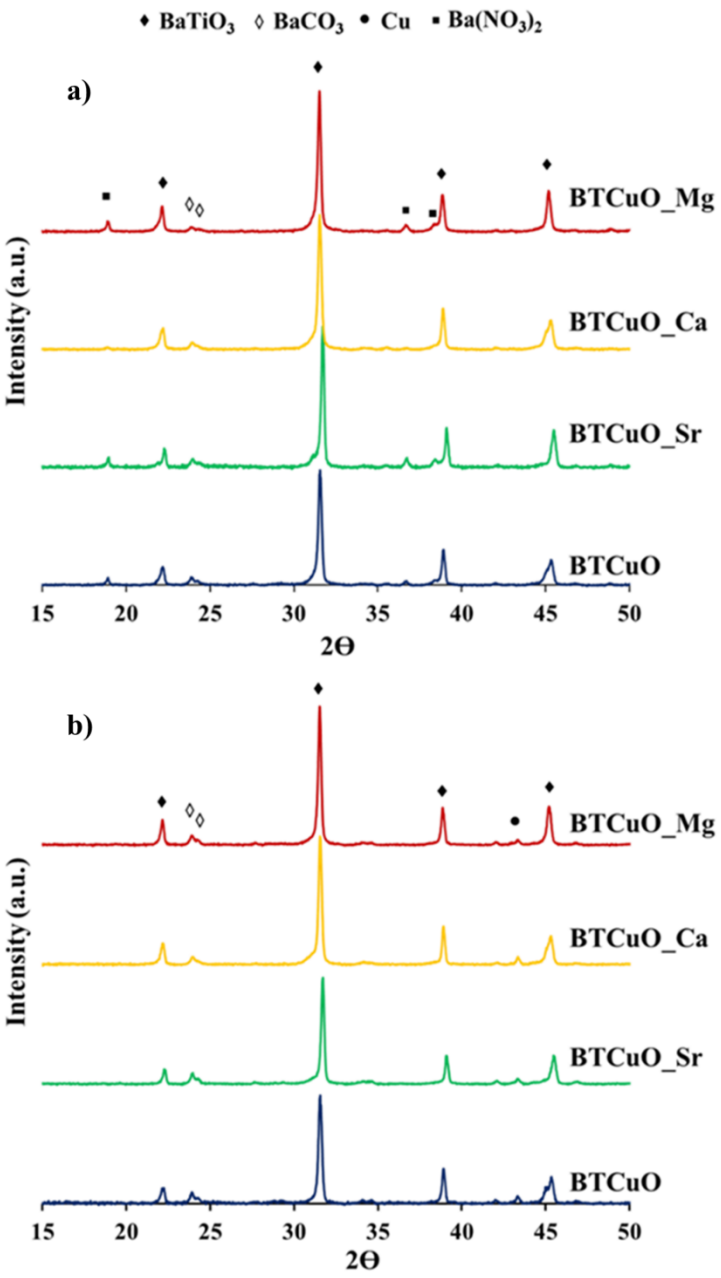
♦ BaTiO3 ◊ BaCO3 • Cu ▪ Ba(NO3)2
a)
BTCuO_Mg
BTCuO_Ca
BTCuO_Sr
BTCuO
Intensity (a.u.)
15 20 25 30 35 40 45 50
2Θ
b)
BTCuO_Mg
BTCuO_Ca
BTCuO_Sr
BTCuO
Intensity (a.u.)
15 20 25 30 35 40 45 50
2Θ

Figure 7.

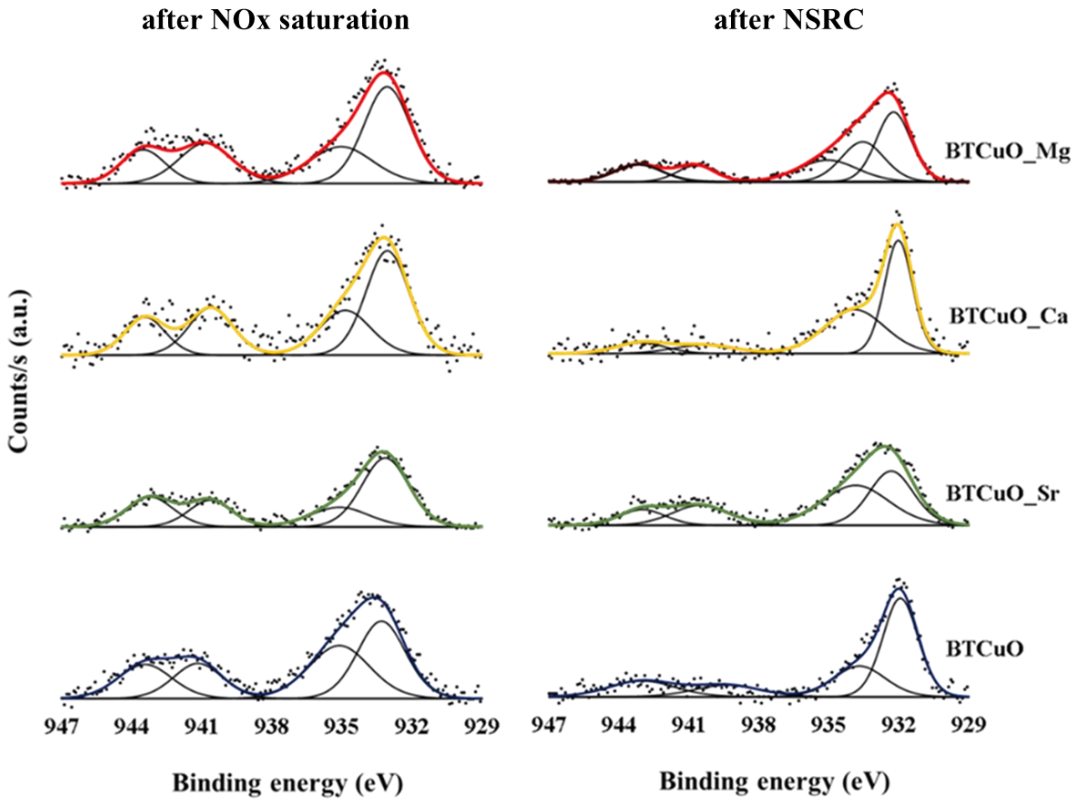
after NOx saturation
after NSRC
BTCuO_Mg
BTCuO_Ca
BTCuO_Sr
BTCuO
Counts/s (a.u.)
947 944 941 938 935 932 929
947 944 941 938 935 932 929
Binding energy (eV)
Binding energy (eV)

Figure 8.

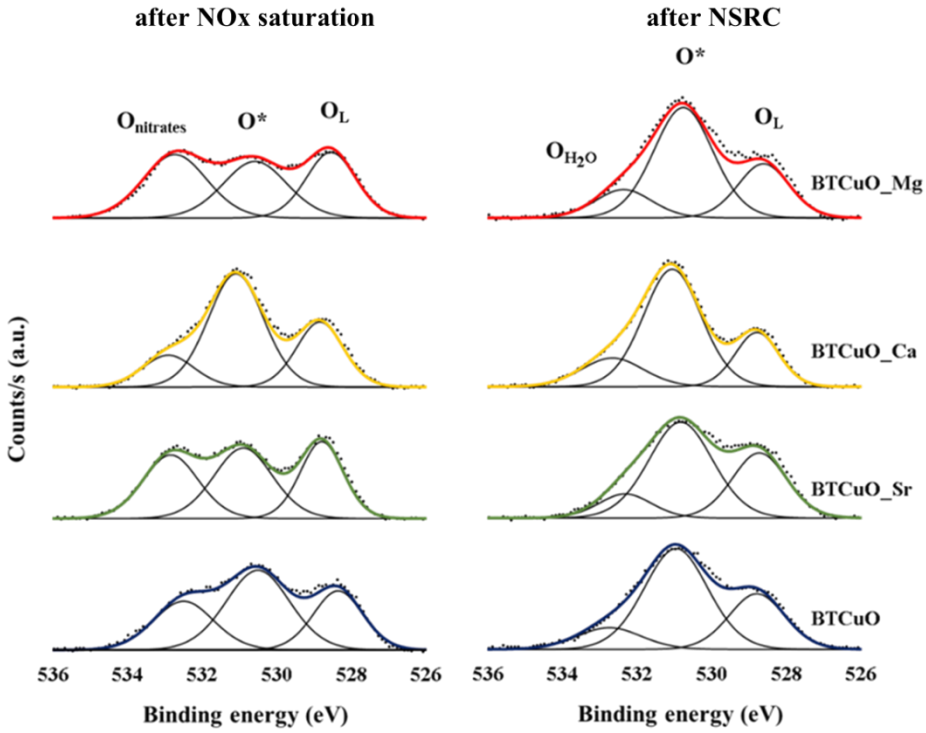
after NOx saturation
after NSRC
O*
$O_{nitrates}$
O*
O_L
O_{H_2O}
O_L
BTCuO_Mg
BTCuO_Ca
BTCuO_Sr
BTCuO
Counts/s (a.u.)
536 534 532 530 528 526
Binding energy (eV)
536 534 532 530 528 526
Binding energy (eV)

Figure 9.

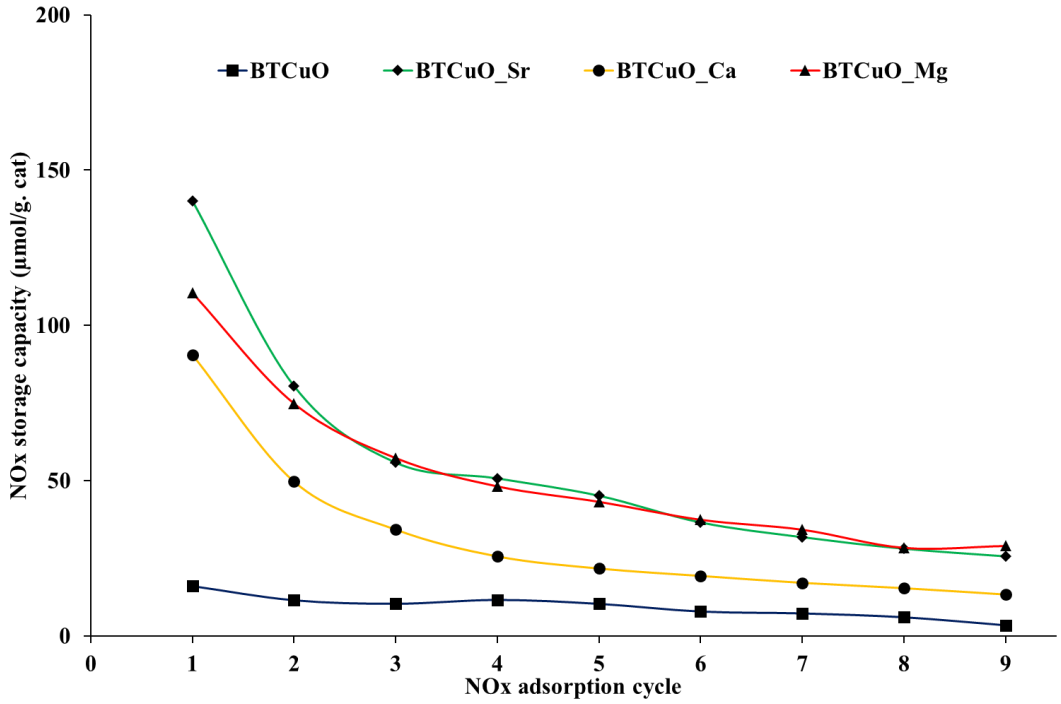
BTCuO
BTCuO_Sr
BTCuO_Ca
BTCuO_Mg
NOx storage capacity (µmol/g. cat)
NOx adsorption cycle
200
150
100
50
0
0
1
2
3
4
5
6
7
8
9

Figure 10.

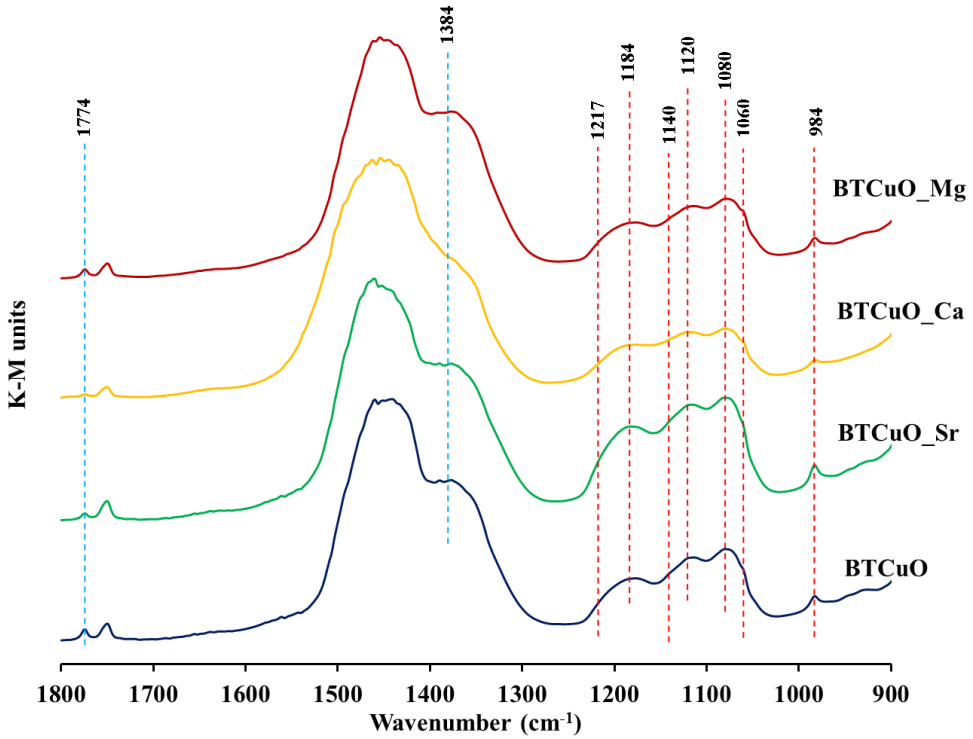
1774
1384
1217
1184
1140
1120
1080
1060
984
BTCuO_Mg
BTCuO_Ca
BTCuO_Sr
BTCuO
K-M units
1800
1700
1600
1500
1400
1300
1200
1100
1000
900
Wavenumber (cm-1)

Figure 11.

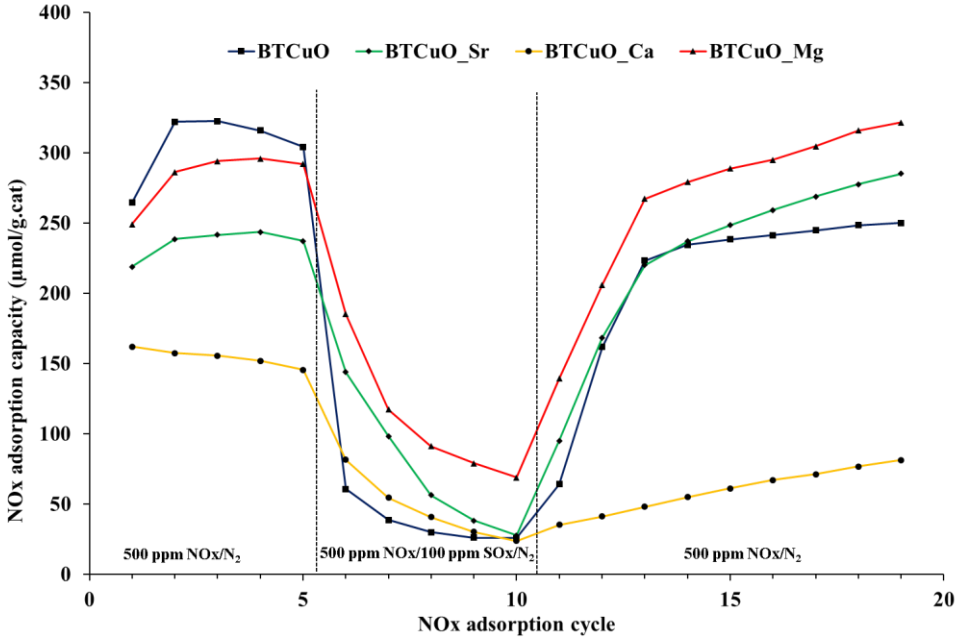
BTCuO
BTCuO_Sr
BTCuO_Ca
BTCuO_Mg
NOx adsorption capacity (µmol/g.cat)
NOx adsorption cycle
500 ppm NOx/N2
500 ppm NOx/100 ppm SOx/N2
500 ppm NOx/N2
0
50
100
150
200
250
300
350
400
0
5
10
15
20

Figure 12.

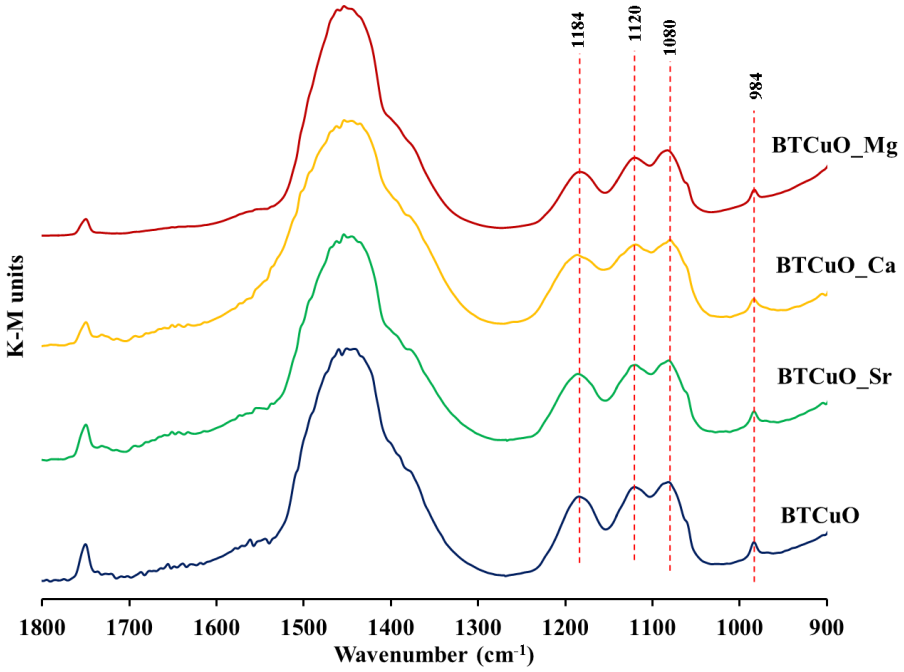
1184
1120
1080
984
BTCuO_Mg
BTCuO_Ca
BTCuO_Sr
BTCuO
K-M units
1800
1700
1600
1500
1400
1300
1200
1100
1000
900
Wavenumber (cm-1)